



HAL
open science

Interfacial organization and phase behavior of mixed galactolipid-DPPC-phytosterol assemblies at the air-water interface and in hydrated mesophases

Jeanne Kergomard, Frédéric Carrière, G. Paboeuf, Franck Artzner, Nathalie Barouh, Claire Bourlieu-Lacanal, V. Vié

► **To cite this version:**

Jeanne Kergomard, Frédéric Carrière, G. Paboeuf, Franck Artzner, Nathalie Barouh, et al.. Interfacial organization and phase behavior of mixed galactolipid-DPPC-phytosterol assemblies at the air-water interface and in hydrated mesophases. *Colloids and Surfaces B: Biointerfaces*, 2022, 217, pp.112646. 10.1016/j.colsurfb.2022.112646 . hal-03702655

HAL Id: hal-03702655

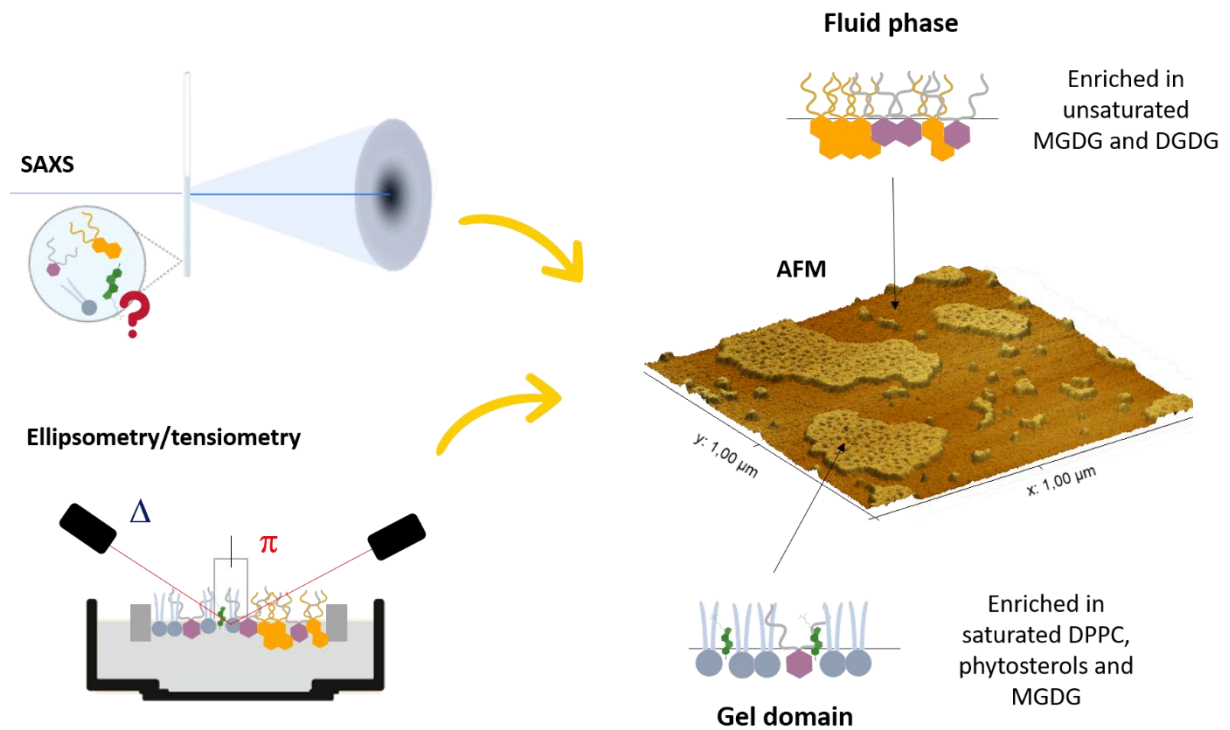
<https://hal.science/hal-03702655v1>

Submitted on 23 Jun 2022

HAL is a multi-disciplinary open access archive for the deposit and dissemination of scientific research documents, whether they are published or not. The documents may come from teaching and research institutions in France or abroad, or from public or private research centers.

L'archive ouverte pluridisciplinaire **HAL**, est destinée au dépôt et à la diffusion de documents scientifiques de niveau recherche, publiés ou non, émanant des établissements d'enseignement et de recherche français ou étrangers, des laboratoires publics ou privés.

1 Graphical abstract



2

3

4 HIGHLIGHTS

- 5 • Plant polar lipids formed stable monolayers at the air/water interface.
- 6 • Phytosterols reduced the lateral elasticity of galactolipid and DPPC monolayer.
- 7 • DPPC has affected MGDG-DGDG interactions.
- 8 • Results highlighted preferential phase miscibility between DPPC and MGDG.

9

10

11 **Title:** Interfacial organization and phase behavior of mixed galactolipid-DPPC-
12 phytosterol assemblies at the air-water interface and in hydrated mesophases

13 **Name(s) of Author(s)** Jeanne Kergomard^{1,2}, Frédéric Carrière³, Gilles Paboeuf¹, Franck Artzner¹,
14 Nathalie Barouh^{4,5}, Claire Bourlieu² & Véronique Vié^{1,6*}

15 **Author Affiliation(s)** ¹ IPR Institute of Physics, UMR UR1 CNRS 6251, Rennes 1 University,
16 France; ²INRAE/CIRAD/UM/Institut Agro Montpellier UMR 1208 IATE, France; ³Aix-Marseille
17 Université, CNRS, UMR7281 Bioénergétique et Ingénierie des Protéines, Marseille, France ;
18 ⁴CIRAD, UMR QUALISUD, F34398 Montpellier-France, ⁵Qualisud, Univ Montpellier,
19 Avignon Université, CIRAD, Institut Agro, Université de La Réunion, Montpellier, France ; ⁶
20 Univ Rennes 1, CNRS, ScanMAT - UMS 2001, F-35042, Renne, France

21 ***Corresponding author: Dr. Véronique Vié, Institut de Physique de Rennes, Campus de**
22 **Beaulieu, UMR UR1 CNRS 6251, Université de Rennes 1, 35042 Rennes cedex, phone number:**
23 033223235645 and E-mail address : veronique.vie@univ-rennes1.fr

24 **Present/permanent address:** Institut de Physique de Rennes, campus de Beaulieu, 35042 Rennes
25 cedex – France

26

27 **Word count: 6272**

28 **Total number of tables/figures: 8**

29

30 **Abbreviations**

31 AFM: atomic force microscopy

32 DGDG: digalactosyldiacylglycerol

33 DPPC: 1,2-dipalmitoyl-sn-glycero-3-phosphocholine

34 GL: galactolipid

35 MGDG: monogalactosyldiacylglycerol

36 PL: phospholipid

37 pS: phytosterol

38 PUFA: polyunsaturated fatty acids

39 SAXS: X-ray scattering

40 **ABSTRACT**

41 The structural behavior of model assemblies composed of monogalactosyldiacylglycerol (MGDG)
42 and digalactosyldiacylglycerol (DGDG), the two main galactolipids found in plants, was
43 investigated at the air/water interface and in aqueous dispersion. To approach the composition of
44 the natural photosynthetic membranes, tunable Langmuir model membrane of galactolipids (GL)
45 were used, and were complexified to form either heterogenous binary or ternary assemblies of GL,
46 phospholipids (PL), and phytosterols (pS).

47 The impact of pS, 1,2-dipalmitoyl-sn-glycero-3-phosphocholine (DPPC) or both on the structural
48 properties of GL membrane was studied. The nature of the interactions between the different
49 molecules was investigated using biophysical characterizations (ellipsometry, tensiometry, atomic
50 force microscopy). In addition, the phase behavior was determined by SAXS analysis on the model
51 assemblies in aqueous dispersions.

52 Results revealed the good interfacial stability of these specific plant membrane lipids. The
53 morphology of the GL film was characteristic of a fluid phase, with an interfacial roughness
54 induced by the intercalation of monogalactosyl and digalactosyl polar heads of MGDG and DGDG,
55 respectively. A phase heterogeneity in the monolayer was induced by the addition of DPPC and/or
56 pS, which resulted in the modification of galactolipid organization and headgroup interactions.
57 These structural changes were confirmed by SAXS analysis, showing more favorable interactions
58 between MGDG and DPPC than between DGDG and DPPC in aqueous dispersion. This
59 phenomenon was exacerbated in the presence of pS.

60

61 **KEYWORDS:** galactolipid, phytosterol, natural surfactant, vegetal photosynthetic assemblies

62 1 INTRODUCTION

63 Galactolipids are the most abundant polar lipids found in higher plants. These glycolipids are
64 actively involved in the structuration of the plant membranes and are particularly concentrated in
65 the photosynthetic chloroplast membranes (80% wt. of total non-pigmented lipids), which contain
66 large amounts of monogalactosyldiacylglycerol (MGDG, 53% wt.) and digalactosyldiacylglycerol
67 (DGDG, 27% wt.) (Gurevich et al., 1997). MGDG possess a small 1- β -galactose polar head bound
68 to a diacylglycerol, giving it a conical shape, which can induce curvatures in lamellar phases (Lee,
69 2000). On the other hand, DGDG has a larger polar head with an additional α -galactose, linked to
70 β -galactose (Mizusawa & Wada, 2012) and adopts a cylindrical shape in solution. Both GL possess
71 two esterified acyl chains at the *sn*-1 and *sn*-2 position of the glycerol backbone, whose molecular
72 motion depends on the number of unsaturation.

73 Due to their different structure, MGDG and DGDG exhibit distinct phase behaviors, which
74 govern the overall membrane architecture (Fig. 1). Indeed, studies on the phase behavior of GL
75 have shown that DGDG forms lamellar phases (L_{α}) and induces bilayer formation, whereas
76 unsaturated MGDG tends to form inverted hexagonal structures (H_{II}) in aqueous solution (Brentel
77 et al., 1985). In addition to their biological functions in photosynthetic membranes, GL are of
78 nutritional interest since they are rich in polyunsaturated fatty acids (PUFA), and their consumption
79 provides essential ω 3 fatty acids (Sahaka et al., 2020).

80 Phytosterols (pS) are also among the major compounds of photosynthetic plant membranes
81 where they play crucial roles in regulating the physical properties of membranes (Evans, 1991;
82 Ostlund, 2002). More than 250 species of phytosterols have been reported, the most abundant being
83 β -sitosterol (70% wt.), stigmasterol (20% wt.) and campesterol (5% wt.) (Evans, 1991). These pS

84 in their free form participate in the structuration of membranes by stabilizing polar lipid bilayers,
85 although to a lesser extent than their cholesterol counterpart in animal cell membranes (Moreau et
86 al., 2002). Beyond their structural properties, phytosterols are also compounds of nutritional and
87 medical importance. Their consumption from fruits and vegetables has been shown to lower the
88 total cholesterol and LDL levels in plasma in humans (St-Onge & Jones, 2003). The interesting
89 structural and nutritional properties of GL and pS have raised interest in their use in various
90 applications, which requires a deep understanding of the organization and interactions of these
91 plant polar lipids.

92 The monolayer behavior of saturated GL has already been extensively studied at the
93 air/water interface (Hoyo et al., 2016; Tomoaia-Cotișel et al., 1989). Nevertheless, it should be
94 noted that GL acyl chains in higher plants are mostly polyunsaturated, and thus less stable since
95 they are more susceptible to oxidation (Tomoala-Cotișel et al., 1983). Monolayer studies have also
96 been performed on GL mixtures with unsaturation indices greater than 1, highlighting the
97 differences in interfacial behavior between saturated and unsaturated GL. Using Langmuir films,
98 Bottier et al. (2007) studied the interfacial behavior of GL from different wheat tissues and
99 highlighted the miscibility of MGDG and DGDG in water but also their tendency to phase
100 separation in mixture. Overall, interface organization and packing were governed by interactions
101 between the sugar polar heads of GL (Bishop et al., 1980), but also depended on their fatty acid
102 composition and the number of unsaturations.

103 The impact of plant sterols in polar lipid bilayers has already been studied extensively,
104 showing that they alter phase transitions and membrane fluidity (Itzhaki et al., 1990; McKersie &
105 Thompson, 1979), depending on their chemical structure and concentration (Kamal &
106 Raghunathan, 2012). The interactions between pS and dipalmitoylphosphatidylcholine (DPPC)

107 have also been studied in model Langmuir films at the air/water interface, and the incorporation of
108 β -sitosterol and stigmasterol into PL monolayers has been shown to increase their packing (Su et
109 al., 2007). Nevertheless, to the best of our knowledge, few results are available today concerning
110 the impact of pS and phospholipids on GL interactions and packing in monolayers.

111 The interfacial properties of MGDG and DGDG, as well as their modulation by DPPC
112 and/or pS in mixed Langmuir monolayers at the air/water interface were studied by ellipsometry,
113 tensiometry and atomic force microscopy (AFM). The phase behavior and physical properties of
114 these mixtures in hydrated mesophases were also studied by small angle X-ray scattering (SAXS)

115

116 **2 EXPERIMENTAL SECTION**

117 **2.1 Lipids**

118 1,2-dipalmitoylphosphatidylcholine (DPPC), monogalactosyldiacylglycerol (MGDG) and
119 digalactosyldiacylglycerol (DGDG) were purchased from Avanti Polar Lipids (see Table S1 in the
120 supplementary material for the fatty acid repartition). Canola phytosterols were a gift from Cognis
121 France (Estarac, France) obtained from desodorization distillates of canola oil. Typical molar
122 composition (calculated from usual normalized GC procedures) was: β -sitosterol (50 mol%),
123 campesterol (40 mol%) and brassicasterol (10 mol%).

124 **2.2. Preparation of multicomponent lipid blends**

125 Simple binary mixture of MGDG and DGDG (60:40, mol/mol) was prepared, namely GL. Ternary
126 and quaternary mixtures of glycerophospholipids, galactolipids and phytosterols (see Table 1 for
127 relative molar composition) were prepared to add some phase heterogeneity and to mimic the
128 composition of natural plant photosynthetic membranes.

129 **2.3 Ellipsometry and surface pressure measurements at the air/water interface**

130 All reported experiments were performed at least in duplicate, using a computer controlled and
131 user-programmable LB Teflon Langmuir trough (KSV Nima, Helsinki, Finland) of 77 cm²,
132 equipped with two mobile barriers, allowing to vary the surface. Before each experiment, the
133 trough was carefully cleaned with ultrapure water and ethanol to get rid of the surface-active
134 residual impurities. The surface pressure was measured using a Wilhelmy balance connected to a
135 microelectronic feedback system (Nima Technology, Cambridge, UK). The values of surface
136 pressure (π) were recorded every 15 s with a precision of 0.2 mN/m. A home-made automated
137 ellipsometer in a “null ellipsometer” configuration was used to carry out the ellipsometric angle

138 (Δ) measurement (Berge & Renault, 1993). The laser beam probed a surface of 1 mm² and a depth
139 of 1 μ m and allowed the qualitative monitoring of the thickness of the lipid monolayer formed at
140 the air/water interface. Values of Δ were recorded every 15 s with a precision of $\pm 0.5^\circ$.

141 **2.3.1 Formation of the lipid monolayers and Langmuir Blodgett transfer**

142 For all the characterizations, the aqueous phase was composed of a 10 mM Tris HCl buffer solution
143 (100 mM NaCl, 5 mM CaCl₂, 10 mM Tris) at pH 7. The monolayers were formed by spreading a
144 few microliters of 1 mM solution of lipids in CHCl₃/MeOH (2:1, v/v) at the air/water interface
145 using a Hamilton microliter syringe. The surface area of the Langmuir trough was set at 35 cm²
146 and the lipids were deposited up to a surface pressure of 20 mN/m. The film was then equilibrated
147 for 10 minutes before each measurement, allowing the evaporation of solvent and lipid organization
148 at the air/water interface. After 10 minutes equilibrium, the interfacial film was transferred onto a
149 freshly cleaved mica plate, using the Langmuir Blodgett method (lipid-transfer ratio ~ 1.0). All
150 lipid layers were sampled at a very low speed (0.5 mm.min⁻¹) by raising vertically the mica plate
151 through the air/water interface. The surface pressure was kept constant during the sampling to
152 maintain the lateral organization of lipids and thus avoid desorption phenomena and interfacial
153 disorganization.

154 **2.3.2 Compression isotherms and compressibility modulus C⁻¹**

155 The surface area of the Langmuir trough was set at 77 cm² before compression. Few microliters of
156 1 mM solution of lipids in CHCl₃/MeOH (2:1, v/v) were spread at the interface until the pressure
157 reaches 0.1 mN/m. The surface pressure as a function the surface area of the trough (π -A isotherm)
158 was then recorded upon a symmetrical compression of the lipid monolayer using the two barriers,
159 from 77 cm² to 21 cm², until the collapse of the film. The barrier speed was set at 5 mm²/min.

160 Compression isotherms allow to obtain several parameters on the behavior of monolayers under
161 compression. The minimum molecular area corresponds to the mean molecular area occupied by
162 the molecules at the collapse of the film and was calculated as the intercept value between the
163 pressure plateau at collapse and the tangent at the end of the π -A isotherm. The lift-off area was
164 determined as the mean molecular area occupied by the molecules when the pressure begins to
165 increase under compression. Finally, the monolayer compressibility was obtained from the first
166 derivate of π -A isotherm and the mean molecular area of lipids deposited at the interface (Gaines
167 & Prigogine, 1966; Smaby et al., 1997). The equation (1) was used to determine the compressibility
168 coefficient (C_s) of the monolayer.

$$169 \quad (1) C_s = -\frac{1}{A} \times \frac{dA}{d\pi}$$

170 where π is the surface pressure and A is the mean molecular area of the lipids forming the
171 monolayer, estimated from the surface of the trough and the amounts of lipids deposited. The
172 reciprocal of compressibility coefficient, the compressibility modulus, i.e., C_s^{-1} was represented as
173 a function of the mean molecular area ($\text{\AA}^2/\text{molecules}$). C_s^{-1} values were obtained at equally spaced
174 surface pressures (0.2 mN/m intervals).

175 **2.4. Topographic visualization of the monolayer interface using atomic force microscopy**

176 Imaging of the films transferred to mica plates was carried out using an AFM (Multimode
177 Nanoscope 5, Bruker, France). The PeakForce Quantitative Nanomechanical Mapping (QNM in
178 air, 20°C) was used in all the experiments. This mode provides high-resolution AFM images of the
179 sample nanoscale surface topography, as well as the modulus and adhesion, at an acquisition speed
180 comparable to the tapping mode. A standard silicon cantilever was used (0.06 N/m, SNL-10,
181 Bruker, France), and the scan rate was set at 1 Hz. The force was minimized during all scans and

182 the scanner size was $100 \times 100 \mu\text{m}^2$. The processed images analyzed by the open-source platform
183 Gwyddion are representative of at least duplicated experiments. The differences of height of the
184 LC and LE domains were assessed by the plot of height profile based on three cross-sections of the
185 image using the software Gwyddion (2.55). For all AFM images, the color scale covers a height
186 range of 15 nm, with the darkest color corresponding to the lowest domains and the lightest color
187 to the highest domains, the fluid background corresponding to zero. A color scale is provided in
188 Figure 3 to facilitate interpretation of the images.

189 **2.5. Determination of the phase behavior of the model lipid mixture in aqueous dispersions** 190 **by SAXS**

191 The phase behavior of the model lipid mixture was investigated in aqueous dispersions using X-
192 ray scattering with a homemade set-up at the Rennes Physique Institute. The X-ray scattering
193 results were collected with a Pilatus 300 K (Dectris, Switzerland), mounted on a microsource X-
194 ray generator GeniX 3D (Xenocs, France) operating at 30 W. The monochromatic CuK α radiation
195 was of $\lambda = 1.541 \text{ \AA}$. The X-ray diffraction patterns were recorded in a reciprocal space $q = (4\pi \cdot$
196 $\sin\theta)/\lambda$ from repetitive distances $q=0.012$ to 1.742 \AA^{-1} . Small Angle X-ray Scattering (SAXS) and
197 Wide-Angle X-ray Scattering (WAXS) regions were used to determine the supramolecular
198 organization (long range order) of the lipid/water systems and the packing of acyl chains (short
199 range order), respectively. The samples were prepared by evaporation of the solvent containing the
200 solubilized lipids and then hydration at 5% wt of the lipid films in a Tris buffer solution pH 7 (0.5
201 mg of lipids hydrated in $10 \mu\text{L}$ of Tris buffer). The samples were then introduced in thin calibrated
202 quartz capillaries ($\text{\O} 1.5 \text{ mm}$, GLAS W. Muller, Berlin, Germany) before being centrifuged and
203 sealed with candle wax. For the analysis, they have been introduced in a capillary holder
204 accommodating 19 capillaries at controlled temperature. The homogeneity of the sample was

205 checked at two y-positions. The analyses were carried out following a heating and cooling
206 temperature ramp from 12 °C to 42 °C and 42 °C to 12 °C, respectively, every 8°C with an exposure
207 time per point of 10 minutes. The results were collected by a homemade program and the positions
208 of Bragg reflections were determined by the Igor Pro 7.0 software (Wavemetrics, US).

209

210 3 RESULTS AND DISCUSSION

211 3.1 Study of the compression isotherms π -A of the GL_x/pS_y systems – influence of the pS 212 concentration

213 The absence of shoulder and/or inflection point on the compression isotherm of the GL
214 mixture (Fig. 2.A) was characteristic of a homogeneous liquid-expanded (LE) single phase, which
215 could be explained by the high unsaturation content of the mixture. Indeed, the unsaturations
216 decreased the intensity of van der Waals interactions between the acyl chains, and could hinder the
217 establishment of a tight packing between GL molecules in the monolayer. The isotherm of the GL
218 film indicated a lift-off area at around $230.8 \pm 1.8 \text{ \AA}^2/\text{molecule}$ ($2.3 \text{ nm}^2/\text{molecule}$) and showed a
219 regular increase of the surface pressure until the collapse of the film at $\pi=39.9 \pm 0.2 \text{ mN/m}$ and at
220 a limiting area of $81.0 \pm 0.6 \text{ \AA}^2/\text{molecule}$ ($0.8 \text{ nm}^2/\text{molecule}$). The evolution of the π -A isotherm
221 of the GL film was consistent with the study of Bottier et al. (2007) on purified wheat MGDG and
222 DGDG monolayers, pure or in mixture. Nevertheless, a higher collapse pressure of 47 mN/m had
223 been obtained for the less unsaturated wheat MGDG/DGDG equimolar mixture, at a lower mean
224 molecular area of $70 \text{ \AA}^2/\text{molecule}$ ($0.7 \text{ nm}^2/\text{molecule}$). This result was not surprising, as unsaturated
225 acyl chains cannot adopt a very tight packing, which explains a larger average molecular area and
226 a lower surface pressure at collapse as the number of unsaturation increases. The presence of
227 unsaturations in the alkyl chains could also explain the significantly lower Cs_{max}^{-1} which was
228 obtained for the GL monolayer in our study (Fig. 2.B) compared to the Cs_{max}^{-1} reported by Hoyo et
229 al. (2016) on the 2:1 mixture of saturated GL (48 versus 247 mN/m respectively). These values
230 were determined for pressure values of interest, between 30 and 40 mN/m , $\pi=35 \text{ mN/m}$ having
231 been proposed as the equivalence surface pressure between lipid monolayers and cellular bilayers
232 (Marsh, 1996, 2007). This decrease in Cs_{max}^{-1} with increasing unsaturation number had also been

233 reported by Gzyl-Malcher, Filek, Makyła, et al. (2008), reflecting the higher lateral elasticity of
234 unsaturated monolayers compared to the saturated ones.

235 The addition of pS in the GL mixture did not significantly impact the surface pressure at
236 the collapse of the film (Fig. 2.A). The addition of 5 and 10 mol% pS to the GL mixture did not
237 significantly impact the limiting area. In contrast, the limiting area was affected by the addition of
238 30 mol% of pS and shifted from 81.0 ± 0.6 to 66.1 ± 0.5 Å²/molecule (0.8 to 0.7 nm²/molecule).
239 The inclusion of pS has also significantly altered the Cs^{-1}_{max} of the monolayers (Fig. 2.B.,
240 logarithmic scale), and this effect was particularly marked in the presence of 30 mol% of pS in the
241 GL mixture. Indeed, a Cs^{-1}_{max} of 85.7 mN/m was reached for the GL₇₀/pS₃₀ blend, compared to
242 72.8 mN/m for the GL₉₀/pS₁₀ and GL₉₅/pS₅ blends and 48.0 mN/m for the pure GL system. The
243 greater impact of phytosterols for a content of 0.3 mol% on the compressibility of the monolayer
244 was consistent with the results presented in Figure 2.D. Indeed, the phase diagram showed a non-
245 ideal behavior of the GL and pS blends, and this effect was even more noticeable for a molar
246 concentration of pS of 30% in the system. The reduction of the mean molecular area at collapse
247 and the increase of Cs^{-1}_{max} with the increase of pS concentration could be attributed either to the
248 condensation of the unsaturated acyl chains or to the reorientation of the sugar polar heads, induced
249 by the presence of the pS molecule, thus decreasing the lateral elasticity of the monolayers (Li et
250 al., 2001). Indeed, the presence of a largely hydrophobic small molecule such as pS will also impact
251 the tilt of the polar heads, which will increase the possibility of packing of the molecules,
252 explaining the non-ideal behavior observed in the case of unsaturated GL monolayers.
253 Nevertheless, the animal counterpart of pS, the cholesterol, was shown to establish weaker
254 interactions with unsaturated lipids, in comparison with saturated lipids (Silvius, 2003), so the

255 addition of DPPC in the mixtures could drastically alter the phenomena observed in GL-pS
256 monolayers (Jurak, 2013).

257 **3.2 Influence of GL, DPPC, and pS interfacial composition on collapse pressure and** 258 **ellipsometric angle values**

259 Ellipsometry combined with tensiometry were used on Langmuir trough to determine the
260 values of surface pressure (π , mN/m), ellipsometric angle (Δ , °) and limiting molecular area
261 ($\text{\AA}^2/\text{molecule}$) at the collapse of mixed heterogenous films with various compositions in GL, DPPC
262 and pS. The values of π and Δ at the collapse of the films are presented in Table 2.

263 The addition of 10 mol% of pS in the GL mixture has induced a clear increase in the film
264 thickness at collapse (8.2 versus $7.3 \pm 0.5^\circ$ for the GL₉₀/pS₁₀ versus GL mixture, respectively),
265 while there was no significant change in collapse pressure, neither in the limiting area. These results
266 tend to indicate that the inclusion of the pS only impacted the orientation of the GL sugar polar
267 heads, and not the acyl chain organization.

268 The addition of 50 mol% DPPC in the GL mixture led to an increase of the collapse surface
269 pressure to $\pi=44.1 \pm 0.2$ mN/m (versus 39.9 ± 0.2 mN/m for the GL monolayer) as well as a shift
270 in the mean molecular area at collapse to $60.4 \pm 1.0 \text{\AA}^2/\text{molecules}$ ($0.6 \text{ nm}^2/\text{molecule}$), versus 81.0
271 $\pm 0.6 \text{\AA}^2/\text{molecule}$ ($0.8 \text{ nm}^2/\text{molecule}$) for the GL monolayer. These results indicated a strong
272 condensing effect of DPPC, which could be explained by the presence of saturated acyl chains and
273 smaller polar head of DPPC, which decreased the steric hindrance. An increase in the film thickness
274 at collapse induced by the presence of DPPC was also observed ($\Delta=8.9^\circ$ vs 7.30° for the GL film),
275 suggesting a reorientation of the sugar polar heads of GL, as well as the formation of condensed
276 domains upon compression (Vié et al., 1998).

277 The addition of phytosterols at 10 mol% in the GL/DPPC film did not induce a significant
278 variation of the collapse pressure (44.4 ± 0.2 mN/m versus 44.1 mN/m for the GL/DPPC) but
279 triggered a shift of the limiting molecular area from 60.4 ± 1.0 to 55.0 ± 1.7 Å²/molecule (0.6 to
280 0.5 nm²/molecule), indicating an increase of the packing in the mixture in presence of pS. This
281 decrease in the limiting area was not expected, given that pS probably interacts preferentially with
282 DPPC than with PUFA-containing GL. Indeed, Botet-Carreras et al. (2019) have studied the impact
283 of cholesterol on homo- and hetero-acids phospholipid monolayers by AFM and AFM-FS,
284 confirming that the effect of cholesterol on unsaturated PL was weaker than the one exerted on
285 saturated PL. Additionally, a variety of biophysical measurements have revealed that sterols have
286 an aversion to PUFA (Huster et al., 1998; Niu & Litman, 2002; Pitman et al., 2004; Wassall et al.,
287 2004), explaining the lower impact of pS in the presence of GL in the GL₉₀/pS₁₀ mixture, which
288 contain a significant amount of PUFA. One possible explanation for such aversion of sterols for
289 PUFA is the high disorder of PUFA acyl chains, which is incompatible with the usual orientation
290 of cholesterol vertically with respect to interface plane. Thus, one can expect a change in the
291 orientation of the sterol backbone (Harroun et al., 2006). Additionally, cholesterol has already been
292 shown to induce order in lipids in fluid phase, whereas it has the opposite effect on lipids present
293 in gel phase (Garcia-Manyes et al., 2010). Given these general effects of sterols and their aversion
294 to PUFA, we were expected a more pronounced disorganization of DPPC molecules than a
295 condensation effect of GL polyunsaturated lipid chains, and thus a larger limiting area for the
296 GL₄₅/DPPC₄₅/pS₁₀ mixture compared to the GL₅₀/DPPC₅₀ mixture. Nevertheless, given the
297 decrease in the limiting area of the mixture in the presence of pS, it is likely that the addition of pS
298 induced GL organization in the presence of DPPC, raising the question of a potential miscibility
299 between DPPC and MGDG and/or DGDG in the presence of pS, reflecting a more complex
300 mixture.

301 **3.3. Characterization by ellipsometry of interfacial films at 20 mN/m**

302 The thickness of the three model systems was determined by ellipsometry at a surface
303 pressure of 20 mN/m. The detailed molar compositions are given in Table 1. The values of
304 ellipsometric angles obtained at 20 mN/m are presented in Table 3. Eight sub-model systems were
305 also prepared to give a better understanding of the organization and interactions between polar
306 lipids at the air/water interface (see supplementary data S1 for the detailed molar compositions and
307 S2 for the ellipsometric angle values at 20 mN/m).

308 An ellipsometric angle of 7.5° was obtained for the mixed GL monolayer at 20 mN/m.,
309 which was identical to the value obtained with DGDG alone and higher than the value for MGDG
310 (7.5 and $6.3 \pm 0.5^\circ$ respectively). This result was expected as the DGDG lipid film has already been
311 shown to be thicker than the MGDG monolayer (Bottier, 2006).

312 The addition of DPPC to GL at a molar fraction of 0.5 did not induce a significant variation
313 in the thickness at 20 mN/m. This result was consistent with the data obtained with the sub-model
314 systems MGDG₅₀/DPPC₅₀ and DGDG₅₀/DPPC₅₀ (6.3 and $7.4 \pm 0.5^\circ$, respectively), in which the
315 addition of DPPC did not induce a significant variation of the ellipsometric angle at 20 mN/m.

316 The addition of pS to the mixed model system of GL and DPPC, at a molar content of 10%,
317 led to a slight decrease of the ellipsometric angle at 20 mN/m, but it was not significant. By
318 comparison, pS induced a clear decrease in the thickness of the MGDG₄₅/DPPC₄₅/pS₁₀ and
319 DGDG₄₅/DPPC₄₅/pS₁₀ sub-model systems (5.5 and $6.0 \pm 0.5^\circ$, respectively), compared to the
320 MGDG₅₀/DPPC₅₀ and DGDG₅₀/DPPC₅₀ systems (6.3 and $7.4 \pm 0.5^\circ$, respectively). However, no
321 significant variation in thickness was obtained for the sub-models MGDG₉₀/pS₁₀ and

322 DGDG₉₀/pS₁₀, in comparison with the pure MGDG and DGDG systems. These results tend to
323 indicate different interactions of pS with GL-DPPC mixed films and pure MGDG and DGDG.

324 In order to better understand the differences in the organization of the different models and
325 sub-models, atomic force microscopy was used to visualize the interface of the films obtained by
326 Langmuir Blodgett sampling.

327 **3.4 Nanoscale topographic visualization of interfacial films at 20 mN/m using atomic force** 328 **microscopy**

329 Figure 3 shows AFM images of the interfacial organization of the three main model
330 monolayers GL, GL₅₀/DPPC₅₀, and GL₄₅/DPPC₄₅/pS₁₀ after their transfer by the Langmuir-
331 Blodgett technique onto a mica plate and at a surface pressure of 20 ± 0.5 mN/m. The scale used
332 was composed of different shades of brown, related to the differences in height in the monolayers.
333 These color variations were correlated with the different tilt values of the lipid molecules and thus
334 provide information on the orientation of the molecules and their physical state.

335 The $5 \times 5 \mu\text{m}^2$ AFM image of the GL system (Fig. 3.A), was characteristic of a homogeneous
336 liquid-expanded (LE) phase without phase separation, consistent with the presence of unsaturated
337 acyl chains in the fluid phase. However, the $1 \times 1 \mu\text{m}^2$ image highlights the presence of surface
338 roughness, with height differences between 2 to 8 Å (0.2 to 0.8 nm) with respect to the baseline. A
339 similar segregation was previously observed by AFM on mixed films of MGDG:DGDG (68:32
340 mol/mol) by Sarkis et al. (2014). Additionally, Bottier et al. (2007) had observed the presence of
341 irregular protrusions of 7 Å (0.7 nm) and 4 Å (0.4 nm) at surface pressures above 25 mN/m on
342 monolayers of pure MGDG or in equimolar mixture with DGDG, respectively. The presence of
343 these protrusions had been attributed to a specific organization of the MGDG polar heads between

344 them or with those of DGDG, this roughness being absent on the AFM images of the DGDG
345 monolayer. Indeed, a particular orientation of DGDG polar heads induced by the interactions
346 between GL had been highlighted by PM-IRRAS data. The assumption was that the
347 monogalactosyl polar head of MGDG could be responsible for the orientation of the digalactosyl
348 group of DGDG parallel to the interface, with the formation of a network of hydrogen bridges
349 between the polar heads and the water molecules at the interface (Kanduc et al., 2017).

350 The addition of DPPC to the system (2) (Fig. 3.B) resulted in the appearance of 1 nm high
351 condensed domains of varying shapes and sizes at the interface ($5 \times 5 \mu\text{m}^2$ image), likely to be
352 enriched in DPPC, given their degree of saturation. Additionally, a loss of the granularity on 1×1
353 μm^2 images suggests changes in the orientation of the galactosyl polar heads of GL, that could
354 result from a modification by DPPC of the interactions between MGDG and DGDG. This would
355 fit with the previous results obtained on the compressibility of the film.

356 The addition of pS to the $\text{GL}_{50}/\text{DPPC}_{50}$ mixture (Fig. 3.C) resulted in a subsequent dilution
357 of the domains in the LC condensed phase, as well as a significant increase in the thickness of the
358 domains ($h=1.6$ nm versus $h=1.0$ nm, with and without pS, respectively), in contrast to the
359 unchanged value of the ellipsometric angle. The irregular domain boundaries also indicated a
360 change in line tension induced upon addition of pS in the GL/DPPC system, and suggests a change
361 in interactions between the different classes of lipids, with miscibility regions between the different
362 components. Defects were also visible at the condensed phase domains, probably induced by the
363 inclusion of pS and the local subsequent disorganization of the saturated acyl chains of DPPC.

364 In order to investigate the composition of the condensed phase domains and to better
365 understand the interactions involved between the different classes of lipids, four sub-model systems
366 were prepared, namely $\text{MGDG}_{50}/\text{DPPC}_{50}$, $\text{DGDG}_{50}/\text{DPPC}_{50}$, $\text{MGDG}_{30}/\text{DPPC}_{60}/\text{pS}_{10}$ and

367 DGDG₃₀/DPPC₆₀/pS₁₀ (mol%) mixtures. AFM images and height profiles of these sub-models are
368 presented Figure 4.

369 In the absence of pS, the 5×5 μm² AFM image of the MGDG₅₀/DPPC₅₀ mixture (Fig. 4.A)
370 showed the presence of LC phase domains (average domain area=0.1 μm²), of irregular shape and
371 1.7 nm height, as well as a background characteristic of a homogeneous fluid phase. The
372 DGDG₅₀/DPPC₅₀ film (Fig. 4.B) presented a similar fluid background. However, the LC phase
373 domains are more abundant but smaller (average domain area=0.0002 μm²), and present a greater
374 height of 1.9 nm, in accordance with the higher ellipsometric angle for this mixture (6.3° versus
375 7.4° for the MGDG₅₀/DPPC₅₀ and DGDG₅₀/DPPC₅₀ mixtures, respectively). These observations
376 confirm the different nature of MGDG and DGDG interactions with DPPC and question a possible
377 segregation of MGDG-DGDG interactions in the presence of DPPC.

378 The addition of pS up to 10 mol% in these two previous sub-model systems changed the
379 appearance of the interfacial films. First, the addition of pS in the MGDG/DPPC system (Fig. 4.C)
380 induced a change in the line tension of the condensed phase domains, which showed irregular edges
381 as well as the presence of defects at the larger domains, probably induced by the presence of pS,
382 similar to the previous observations on the model systems. Nevertheless, a significant decrease of
383 18% in the height of these domains (1.7 nm vs. 1.4 nm in height, without and with pS, respectively)
384 was observed, consistent with the evolution of the ellipsometric angle (6.3° vs. 5.5°, without and
385 with pS, respectively). The addition of pS in the DGDG/DPPC mixture induced a similar evolution
386 of the interface (Fig. 4.D): the line tension and the thickness of the condensed domains were also
387 modified according to the same trend (16% decrease in thickness), and the presence of defects at
388 the larger domains with irregular edges was still visible. This change in thickness did not showed

389 the same trend as that observed in the $GL_{45}/DPPC_{45}/pS_{10}$ model, for which a 45% increase in
390 domain thickness was observed.

391 Overall, the results confirm the hypotheses of a different miscibility between DPPC and MGDG
392 and between DPPC and DGDG. Moreover, it seems that the inclusion of pS in the systems induced,
393 on the one hand, a transition from the DPPC-enriched gel phase to a less ordered phase, with the
394 apparition of defects, and on the other hand, a transition from a fluid phase to a less ordered zone,
395 with reduced height mismatch and a decrease of the line tension in the ternary systems. To validate
396 these hypotheses and determine the miscibility of DPPC in mixture with MGDG or DGDG, as well
397 as the impact of pS in $GL/DPPC$ lipid systems, SAXS experiments were performed, in the presence
398 of water in excess.

399

400 **3.5. Phase behavior of mixed galactolipid mixtures in hydrated mesophase (SAXS)**

401 The three-dimensional structures of unsaturated MGDG and DGDG, alone or in their
402 equimolar mixture, have already been studied by analysis of the X-ray diffraction patterns and
403 electron density profile at 20°C in excess of water (Bottier et al., 2007; Hoyo et al., 2016). On one
404 hand, the lamellar structure L_{α} of DGDG was evidenced by the presence of single peaks regularly
405 spaced, with a lamellar periodicity of 54.9 Å. On the other hand, the X-ray diffraction profile
406 obtained for MGDG showed six Bragg diffraction pics, with a hexagonal periodicity of 67.2 Å,
407 that were attributed to an inverse hexagonal phase (H_{II}) distribution, which has been observed in
408 other studies over a wide temperature range (-15 to 80°C) (Popova & Hinch, 2011). The ability
409 of unsaturated MGDG to form non-lamellar structures can be neutralized by mixing it with at least
410 50% of lipids forming lamellar phases. However, unsaturated MGDG can induce defects in the
411 lamellar structure of MGDG/lipid mixtures forming bilayers when its proportion is between 20 and
412 50% (Castro et al., 2007). Nevertheless, for the equimolar mixture of MGDG and DGDG in excess
413 of water, the SAXS diffraction pattern obtained by Bottier et al. was the signature of a bicontinuous
414 cubic phase ($Im3m$ space group) with a cubic lattice parameter of 202 Å, showing the specific
415 behavior of MGDG and DGDG in the equimolar mixture compared to the pure lipids. Indeed, the
416 formation of an $Im3m$ space group could result from specific interactions between the polar sugar
417 heads of the MGDG and DGDG.

418 The three-dimensional organization of DPPC has also already been extensively studied by
419 SAXS, showing a well-ordered multilayer structure in excess of water due to the so-called L_{β} gel
420 phase at 20°C (Et-Thakafy et al., 2017; Varga et al., 2007). Nevertheless, the miscibility of the
421 mixture of GL with DPPC forming lamellar phases has never been studied by SAXS.

422 First of all, the present study investigated the three-dimensional organization of
423 heterogenous $GL_x/DPPC_y$ mixtures in excess of water, and as a function of DPPC proportion.
424 Figure 5.A presented the X-Ray diffraction patterns of three mixtures of $GL_x/DPPC_y$ in water, with
425 DPPC at 66 (black curve), 50 (blue curve), and 33 mol% (green curve), respectively. The results
426 showed that DPPC in large amount of 66 mol% induced a segregation between the components in
427 water. Indeed, on the diffraction pattern (black line), the large diffraction peaks visible at 0.09 and
428 0.18 \AA^{-1} were identified as the ones related to the L_β phase formed by pure DPPC at 20°C .
429 Additionally, a peak and a shoulder were visible on the diffraction pattern at 0.06 and 0.11 \AA^{-1} ,
430 respectively, that could correspond to the diffraction pattern of the cubic phase of the MGDG-
431 DGDG mixture in water, consistent with the results of Bottier et al. (2007). These results tend to
432 indicate a segregation between DPPC and the MGDG-DGDG mixture in water, leading to the
433 existence of two non-miscible phases. Nevertheless, DPPC may also have disrupted the cubic phase
434 by diluting the MGDG-DGDG interactions, coinciding with the distorted pattern of the MGDG-
435 DGDG cubic phase. When DPPC was added at 50 mol% in the GL mixture, the diffraction pattern
436 (blue line) showed a better miscibility between the three components of the system. Indeed, the
437 intensity of the peaks presumably related to the cubic phase of the GL mixture was decreased and
438 the pic 0.06 \AA^{-1} was no longer visible, tending to show the existence of two miscible phases. These
439 results were consistent with AFM images of the $GL_{50}DPPC_{50}$ mixture, where a fluid phase was
440 visible, probably composed of a mixture of MGDG, DGDG and DPPC, as well as condensed
441 domains, likely enriched in DPPC. At a ratio of 33 mol% DPPC, the diffraction pattern (green line)
442 indicates that the concentration of DPPC was not sufficient enough to segregate the three
443 components of the system, and the slightly weaker MGDG-DGDG interactions have probably
444 prevailed, leading to the existence of a single organized phase composed by MGDG, DGDG and

445 DPPC. Overall, the SAXS data confirm the presence of significant segregation in the systems,
446 depending on the DPPC proportion and implying the existence of very selective interactions
447 between the different types of lipids.

448 To our knowledge, this study is the first on the impact of pS on heterogenous model plant
449 membranes, while the impact of cholesterol on model of animal membranes made of phospholipid
450 bilayers has been extensively studied. To better understand the impact of pS and the interactions
451 between DPPC and MGDG/DGDG, the SAXS diffraction patterns of three other model systems
452 were studied, *i.e.* MGDG₄₅DPPC₄₅pS₁₀, GL₄₅/DPPC₄₅/pS₁₀ and DGDG₄₅/DPPC₄₅/pS₁₀ (fig. 5.B).

453 On one hand, results tend to show that MGDG and DGDG did not interact equivalently
454 with the DPPC-pS mixture. First of all, the mixture of DGDG with DPPC-pS did not promote the
455 presence of a single organized phase in water (see green line). Indeed, the diffraction pattern of the
456 pure DPPC was clearly visible, with the L_β lamellar phase peaks at 0.09, 0.18, and 0.27 Å⁻¹. The
457 diffraction pattern of the pure DGDG was also clearly evidenced, with the diffraction peaks
458 reflecting the L_α phase at 0.11 and 0.22 Å⁻¹. These results are consistent with those obtained by
459 Bottier et al. (2007) on the wheat DGDG/water system and they highlight the poor miscibility of
460 DGDG with DPPC-pS system. On the contrary, in the case of the MGDG₄₅/DPPC₄₅/pS₁₀ mixture
461 (blue pattern), only one phase was clearly visible, with two peaks reflecting a lamellar phase at
462 0.09 and 0.18 Å⁻¹, but slightly shifted compared to pure DPPC in water. In the case of the
463 GL₄₅/DPPC₄₅/pS₁₀ mixture in water (black pattern), a shoulder was also visible at 0.11 Å⁻¹,
464 compared to the diffraction pattern of the MGDG₄₅/DPPC₄₅/pS₁₀ mixture, highlighting the
465 formation of two phases: one phase enriched in MGDG-DPPC-pS and one phase containing a
466 mixture of MGDG-DGDG. These results showed drastically different interactions between MGDG

467 and DGDG, respectively, and the DPPC-pS mixture, and highlight the preferential miscibility of
468 MGDG with the DPPC-pS mixture.

469 On the other hand, the comparison between the GL₅₀/DPPC₅₀ (fig. 5. A, blue pattern) and
470 the GL₄₅/DPPC₄₅/pS₁₀ (fig. 5. B, black pattern) mixtures in water allowed us to highlight the impact
471 of 10 mol% of pS in the system. As expected, pS did not form a phase on its own but triggered
472 a modification of the organization of the existing phases. Indeed, the inclusion of pS in the
473 GL/DPPC system did not induce the appearance of new diffraction peaks, but has led to a
474 contraction of the L_β diffraction peaks at 0.09 and 0.18 Å⁻¹, indicating a homogenization in the
475 miscibility of the two phases.

476 Overall, the results were consistent with the AFM images obtained on the
477 GL₄₅/DPPC₄₅/pS₁₀ monolayer, with the visualization of a fluid phase composing the background,
478 probably enriched in MGDG-DGDG, and the presence of a gel phase enriched in MGDG-DPPC,
479 in which the inclusion of pS has induced the formation of defects, leading to a thickening of the
480 gel phase by decreasing the packing. Additionally, the observation of smaller domains in presence
481 of pS on the AFM images was consistent with a lowering of the line tension at the edges of the gel
482 domains, resulting from a better miscibility between the two phases and thus a reduced height
483 mismatch.

484

485 CONCLUSION

486 In this study, tunable Langmuir model membrane of heterogenous assemblies of GL, DPPC and
487 pS were used to study the structural behavior of the main polar lipids of vegetal photosynthetic
488 membrane (MGDG and DGDG) at the air/water interface. The impact of pS and 1,2-dipalmitoyl-
489 sn-glycero-3-phosphocholine (DPPC) or both on the structural properties of GL membrane was
490 studied.

491 The biophysical results obtained confirmed the good surfactant properties of these polar lipids. The
492 addition of pS in the mixed GL systems up to 30 mol% induced a reorientation of the sugar polar
493 heads, leading to a more important packing and thus to a reduction of the lateral elasticity of the
494 monolayer. The study of the compressibility isotherms of the different films also allowed to
495 highlight the complex miscibility of the heterogeneous ternary mixtures, and their singular
496 behavior compared to the pure systems. Indeed, the results obtained on the GL₄₅/DPPC₄₅/pS₁₀
497 mixture indicated preferential DPPC-pS interactions but a decrease in lateral elasticity despite the
498 disorganization effect of pS on saturated lipids.

499 The inclusion of pS into the gel phase regions was visible on the AFM images, leading to a
500 thickening of the domains and a local decrease of packing by the appearance of defects. This result
501 highlighted phase miscibility between DPPC and GL, and in particular with MGDG, which was
502 confirmed by AFM images and SAXS diffraction patterns. The favorable interaction between
503 DPPC and pS may have caused the appearance of segregated zones, on one side, devoid of pS and
504 enriched in MGDG-DGDG in the fluid phase, and on the other, enriched in pS and DPPC.

505 The pS-DPPC-rich areas could also have included the presence of MGDG, due to more favorable
506 DPPC-MGDG interactions than DPPC-DGDG, raising the hypothesis of a heterogeneous MGDG-

507 DPPC-pS composition of the gel phase domains. The characterization of these kinds of plant lipid
508 mixtures is useful for the understanding of mechanisms such as their digestion by specific digestive
509 enzymes.

510 **Declaration of Competing Interest**

511 The authors declare that they have no known competing financial interests or personal relationships
512 that could have appeared to influence the work reported in this paper.

513

514 **Acknowledgments**

515 The authors would like to acknowledge the BIOMIF platform ('Biological Molecules at fluid
516 interfaces', IPR, Rennes, France) for allowing the biophysical characterization of samples
517 presented in this article.

518 C. Bourlieu, V. Vié and J. Kergomard determined the outline and the content of the manuscript. J.
519 Kergomard wrote the manuscript and all the co-authors participated in the experimental design, the
520 collection, the interpretation of data and the correction and implementation of the manuscript. All
521 co-authors have approved the final article.

522

523 **References**

- 524 Berge, B., & Renault, A. (1993). Ellipsometry Study of 2D Crystallization of 1-Alcohol
525 Monolayers at the Water Surface. *Europhysics Letters (EPL)*, *21*(7), 773-777.
526 <https://doi.org/10.1209/0295-5075/21/7/010>
- 527 Bishop, D. G., Kenrick, J. R., Bayston, J. H., Macpherson, A. S., & Johns, S. R. (1980). Monolayer
528 properties of chloroplast lipids. *Biochimica et Biophysica Acta (BBA) - Biomembranes*,
529 *602*(2), 248-259. [https://doi.org/10.1016/0005-2736\(80\)90308-9](https://doi.org/10.1016/0005-2736(80)90308-9)
- 530 Botet-Carreras, A., Montero, M. T., Domènech, Ò., & Borrell, J. H. (2019). Effect of cholesterol
531 on monolayer structure of different acyl chained phospholipids. *Colloids and Surfaces B:*
532 *Biointerfaces*, *174*, 374-383. <https://doi.org/10.1016/j.colsurfb.2018.11.040>
- 533 Bottier, C. (2006). *Caractérisation des puroindolines, des galactolipides du blé et de leurs*
534 *interactions : Mesures physiques aux interfaces* [Phdthesis, Université Rennes 1].
535 <https://tel.archives-ouvertes.fr/tel-00148405>
- 536 Bottier, C., Géan, J., Artzner, F., Desbat, B., Pézolet, M., Renault, A., Marion, D., & Vié, V. (2007).
537 Galactosyl headgroup interactions control the molecular packing of wheat lipids in
538 Langmuir films and in hydrated liquid-crystalline mesophases. *Biochimica Et Biophysica*
539 *Acta*, *1768*(6), 1526-1540. <https://doi.org/10.1016/j.bbamem.2007.02.021>
- 540 Brentel, I., Selstam, E., & Lindblom, G. (1985). Phase equilibria of mixtures of plant galactolipids.
541 The formation of a bicontinuous cubic phase. *Biochimica et Biophysica Acta (BBA) -*
542 *Biomembranes*, *812*(3), 816-826. [https://doi.org/10.1016/0005-2736\(85\)90277-9](https://doi.org/10.1016/0005-2736(85)90277-9)
- 543 Castro, V., Dvinskikh, S. V., Widmalm, G., Sandström, D., & Maliniak, A. (2007). NMR studies
544 of membranes composed of glycolipids and phospholipids. *Biochimica et Biophysica Acta*

545 (BBA) - *Biomembranes*, 1768(10), 2432-2437.
546 <https://doi.org/10.1016/j.bbamem.2007.05.010>

547 Et-Thakafy, O., Delorme, N., Gaillard, C., Mériadec, C., Artzner, F., Lopez, C., & Guyomarc'h, F.
548 (2017). Mechanical Properties of Membranes Composed of Gel-Phase or Fluid-Phase
549 Phospholipids Probed on Liposomes by Atomic Force Spectroscopy. *Langmuir*, 33(21),
550 5117-5126. <https://doi.org/10.1021/acs.langmuir.7b00363>

551 Evans, C. S. (1991). J. B. Harborne (ED.) *Methods in plant biochemistry: 1. plant phenolics*.
552 Academic Press, New York and London, 1990. *Phytochemical Analysis*, 2(1), 48-48.
553 <https://doi.org/10.1002/pca.2800020110>

554 Gaines, G. L., & Prigogine, I. P. (1966). *Insoluble monolayers at liquid-gas interfaces*.

555 Garcia-Manyes, S., Redondo-Morata, L., Oncins, G., & Sanz, F. (2010). Nanomechanics of Lipid
556 Bilayers: Heads or Tails? *Journal of the American Chemical Society*, 132(37),
557 12874-12886. <https://doi.org/10.1021/ja1002185>

558 Gurevich, V., Bondarenko, B., Gundermann, K. J., Schumacher, R., Astashkina, T., Ivanov, V.,
559 Popov, Y., Shatilina, L., & Kazennova, N. (1997). Poly-unsaturated phospholipids increase
560 the hypolipidemic effect of Lovastatin. *European Journal of Internal Medicine*, 8(1), 15-20.

561 Gzyl-Malcher, B., Filek, M., Makyła, K., & Paluch, M. (2008). Differences in surface behaviour
562 of galactolipoids originating from different kind of wheat tissue cultivated in vitro.
563 *Chemistry and Physics of Lipids*, 155(1), 24-30.
564 <https://doi.org/10.1016/j.chemphyslip.2008.06.004>

565 Hoyo, J., Gaus, E., & Torrent-Burgués, J. (2016). Monogalactosyldiacylglycerol and
566 digalactosyldiacylglycerol role, physical states, applications and biomimetic monolayer
567 films. *The European Physical Journal E*, 39(3), 39. <https://doi.org/10.1140/epje/i2016->
568 16039-0

569 Itzhaki, H., Borochoy, A., & Mayak, S. (1990). Age-Related Changes in Petal Membranes from
570 Attached and Detached Rose Flowers. *Plant Physiology*, *94*(3), 1233-1236.

571 Jurak, M. (2013). Thermodynamic Aspects of Cholesterol Effect on Properties of Phospholipid
572 Monolayers : Langmuir and Langmuir–Blodgett Monolayer Study. *The Journal of Physical
573 Chemistry B*, *117*(13), 3496-3502. <https://doi.org/10.1021/jp401182c>

574 Kanduc, M., Schlaich, A., de Vries, A. H., Jouhet, J., Marechal, E., Deme, B., Netz, R. R., &
575 Schneck, E. (2017). Tight cohesion between glycolipid membranes results from balanced
576 water-headgroup interactions. *Nature Communications*, *8*, 14899.
577 <https://doi.org/10.1038/ncomms14899>

578 Lee, A. G. (2000). Membrane lipids : It's only a phase. *Current Biology*, *10*(10), R377-R380.
579 [https://doi.org/10.1016/S0960-9822\(00\)00477-2](https://doi.org/10.1016/S0960-9822(00)00477-2)

580 Li, X.-M., Momsen, M. M., Smaby, J. M., Brockman, H. L., & Brown, R. E. (2001). Cholesterol
581 Decreases the Interfacial Elasticity and Detergent Solubility of Sphingomyelins.
582 *Biochemistry*, *40*(20), 5954-5963. <https://doi.org/10.1021/bi002791n>

583 Marsh, D. (1996). Lateral pressure in membranes. *Biochimica et Biophysica Acta (BBA) - Reviews
584 on Biomembranes*, *1286*(3), 183-223. [https://doi.org/10.1016/S0304-4157\(96\)00009-3](https://doi.org/10.1016/S0304-4157(96)00009-3)

585 Marsh, D. (2007). Lateral Pressure Profile, Spontaneous Curvature Frustration, and the
586 Incorporation and Conformation of Proteins in Membranes. *Biophysical Journal*, *93*(11),
587 3884-3899. <https://doi.org/10.1529/biophysj.107.107938>

588 McKersie, B. D., & Thompson, J. E. (1979). Influence of Plant Sterols on the Phase Properties of
589 Phospholipid Bilayers 1. *Plant Physiology*, *63*(5), 802-805.

590 Mizusawa, N., & Wada, H. (2012). The role of lipids in photosystem II. *Biochimica et Biophysica
591 Acta (BBA) - Bioenergetics*, *1817*(1), 194-208.
592 <https://doi.org/10.1016/j.bbabi.2011.04.008>

593 Moreau, R. A., Whitaker, B. D., & Hicks, K. B. (2002). Phytosterols, phytostanols, and their
594 conjugates in foods : Structural diversity, quantitative analysis, and health-promoting uses.
595 *Progress in Lipid Research*, 41(6), 457-500. [https://doi.org/10.1016-s0163-](https://doi.org/10.1016/s0163-7827(02)00006-1)
596 7827(02)00006-1

597 Popova, A. V., & Hinch, D. K. (2011). Thermotropic phase behavior and headgroup interactions
598 of the nonbilayer lipids phosphatidylethanolamine and monogalactosyldiacylglycerol in the
599 dry state. *BMC Biophysics*, 4(1), 11. <https://doi.org/10.1186/2046-1682-4-11>

600 Sahaka, M., Amara, S., Wattanakul, J., Gedi, M. A., Aldai, N., Parsiegl, G., Lecomte, J.,
601 Christeller, J. T., Gray, D., Gontero, B., Villeneuve, P., & Carrière, F. (2020). The digestion
602 of galactolipids and its ubiquitous function in Nature for the uptake of the essential α -
603 linolenic acid. *Food & Function*. <https://doi.org/10.1039/D0FO01040E>

604 Sarkis, J., Rocha, J., Maniti, O., Jouhet, J., Vié, V., Block, M. A., Breton, C., Maréchal, E., &
605 Girard-Egrot, A. (2014). The influence of lipids on MGD1 membrane binding highlights
606 novel mechanisms for galactolipid biosynthesis regulation in chloroplasts. *The FASEB*
607 *Journal*, 28(7), 3114-3123. <https://doi.org/10.1096/fj.14-250415>

608 Silvius, J. R. (2003). Role of cholesterol in lipid raft formation : Lessons from lipid model systems.
609 *Biochimica Et Biophysica Acta*, 1610(2), 174-183. [https://doi.org/10.1016/s0005-](https://doi.org/10.1016/s0005-2736(03)00016-6)
610 2736(03)00016-6

611 Smaby, J. M., Momsen, M. M., Brockman, H. L., & Brown, R. E. (1997). Phosphatidylcholine acyl
612 unsaturation modulates the decrease in interfacial elasticity induced by cholesterol.
613 *Biophysical Journal*, 73(3), 1492-1505. [https://doi.org/10.1016/S0006-3495\(97\)78181-5](https://doi.org/10.1016/S0006-3495(97)78181-5)

614 St-Onge, M.-P., & Jones, P. J. H. (2003). Phytosterols and human lipid metabolism : Efficacy,
615 safety, and novel foods. *Lipids*, 38(4), 367-375. [https://doi.org/10.1007/s11745-003-1071-](https://doi.org/10.1007/s11745-003-1071-3)

616 3

617 Su, Y., Li, Q., Chen, L., & Yu, Z. (2007). Condensation effect of cholesterol, stigmasterol, and
618 sitosterol on dipalmitoylphosphatidylcholine in molecular monolayers. *Colloids and*
619 *Surfaces A: Physicochemical and Engineering Aspects*, 293(1), 123-129.
620 <https://doi.org/10.1016/j.colsurfa.2006.07.016>

621 Tomoaia-Cotișel, M., Zsako, J., Chifu, E., & Quinn, P. J. (1989). Hysteresis in compression-
622 expansion cycles of distearoylmonogalactosylglycerol monolayers. *Chemistry and Physics*
623 *of Lipids*, 50(2), 127-133. [https://doi.org/10.1016/0009-3084\(89\)90036-4](https://doi.org/10.1016/0009-3084(89)90036-4)

624 Varga, Z., Bóta, A., & Goerigk, G. (2007). Localization of dihalogenated phenols in vesicle
625 systems determined by contrast variation X-ray scattering. *Journal of Applied*
626 *Crystallography*, 40(s1), s205-s208. <https://doi.org/10.1107/S0021889807001987>

627

628

629 **FIGURES**

630 Figure captions.

631 **Figure 1** Molecular structure and phase behaviour of A) monogalactodiacylglycerol (MGDG) and
632 B) digalactosyldiacylglycerol (DGDG). L α standing for lamellar phase and HII standing for
633 hexagonal inverted phase.

634 **Figure 2** Compression isotherms of 1) GL (red), 2) GL₉₅/pS₅ (deep blue), 3) GL₉₀/pS₁₀ (green), 4)
635 GL₇₀/pS₃₀ (black) monolayers at the air/water interface. A) The graph corresponds to the evolution
636 of π (mN/m) as a function of the mean molecular area ($\text{\AA}^2/\text{molecules}$). B) The graph corresponds
637 to the evolution of the surface compressibility moduli (C_s^{-1} , calculated following the equation (1)),
638 as a function of π (mN/m) of 1), 2), 3) and 4). C) The graph corresponds to the evolution of π
639 (mN/m) as a function of the mean molecular area ($\text{\AA}^2/\text{molecules}$) of the pure pS system. D) The
640 graph corresponds to the mean molecular area ($\text{\AA}^2/\text{molecules}$) at 20 mN/m of each monolayer as a
641 function of the percentage of pS in the systems (pure pS monolayer in light blue). The experiments
642 were performed using Tris HCl buffer at pH 7 and were done in duplicate. Values of π were given
643 with a standard deviation on duplicate measurements of ± 0.2 mN/m.

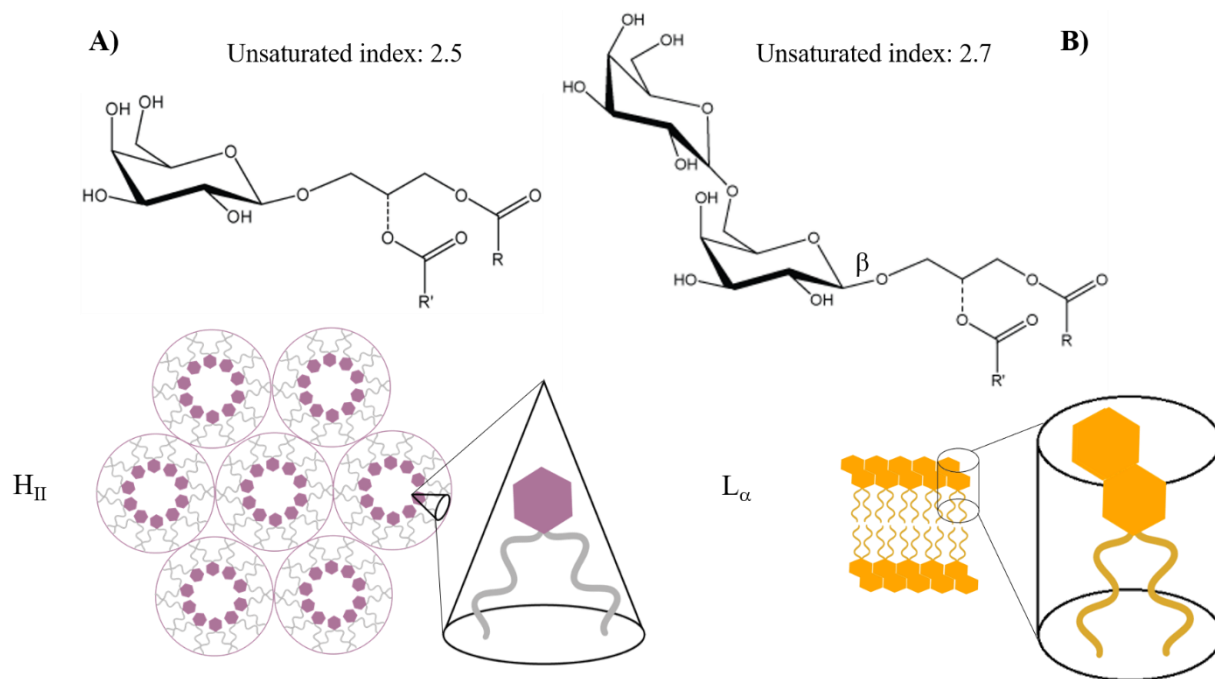
644 **Figure 3** 5x5 μm^2 and 1x1 μm^2 AFM topographic images of A) GL, B) GL₅₀/DPPC₅₀, and C)
645 GL₄₅/DPPC₄₅/pS₁₀ model monolayers. The height profiles were performed on a cross-section of the
646 1x1 μm^2 image. The Langmuir films were transfer at a surface pressure of 20 ± 0.5 mN/m on a
647 mica plate using the Langmuir Blodgett method. Experiments were performed in a Tris HCl buffer
648 at pH 7 and done in duplicate.

649 **Figure 4** 5x5 μm^2 AFM topographic images of A) MGDG₅₀/DPPC₅₀, B) DGDG₅₀/DPPC₅₀, C)
650 MGDG₃₀/DPPC₆₀/pS₁₀, and D) DGDG₃₀/DPPC₆₀/pS₁₀ monolayers. Zooms to 1x1 μm^2 were
651 performed on samples C) and D) to allow visualization of defects in condensed areas. The height
652 profiles were performed on three different cross-sections of the 5x5 μm^2 image. The Langmuir
653 films were transfer at a surface pressure of 20 ± 0.5 mN/m on a mica plate using the Langmuir
654 Blodgett method. The ellipsometric angle value at 20 mN/m was reported to compare the thickness
655 between the four monolayers. Experiments were performed in a Tris HCl buffer at pH 7 and done
656 in duplicate.

657 **Figure 5** SAXS patterns of the model systems recorded at $20 \pm 0.5^\circ\text{C}$. A) GL/DPPC systems at
658 different ratios: 33:67 mol/mol (black curve), 50:50 mol/mol (blue curve) and 67:33 mol/mol
659 (green curve). B) DGDG/DPPC/pS (45:45:10 mol/mol/mol, green curve), GL/DPPC/pS (45:45:10
660 mol/mol/mol, black curve), MGDG/DPPC/pS (45:45:10 mol/mol/mol, blue curve)

661

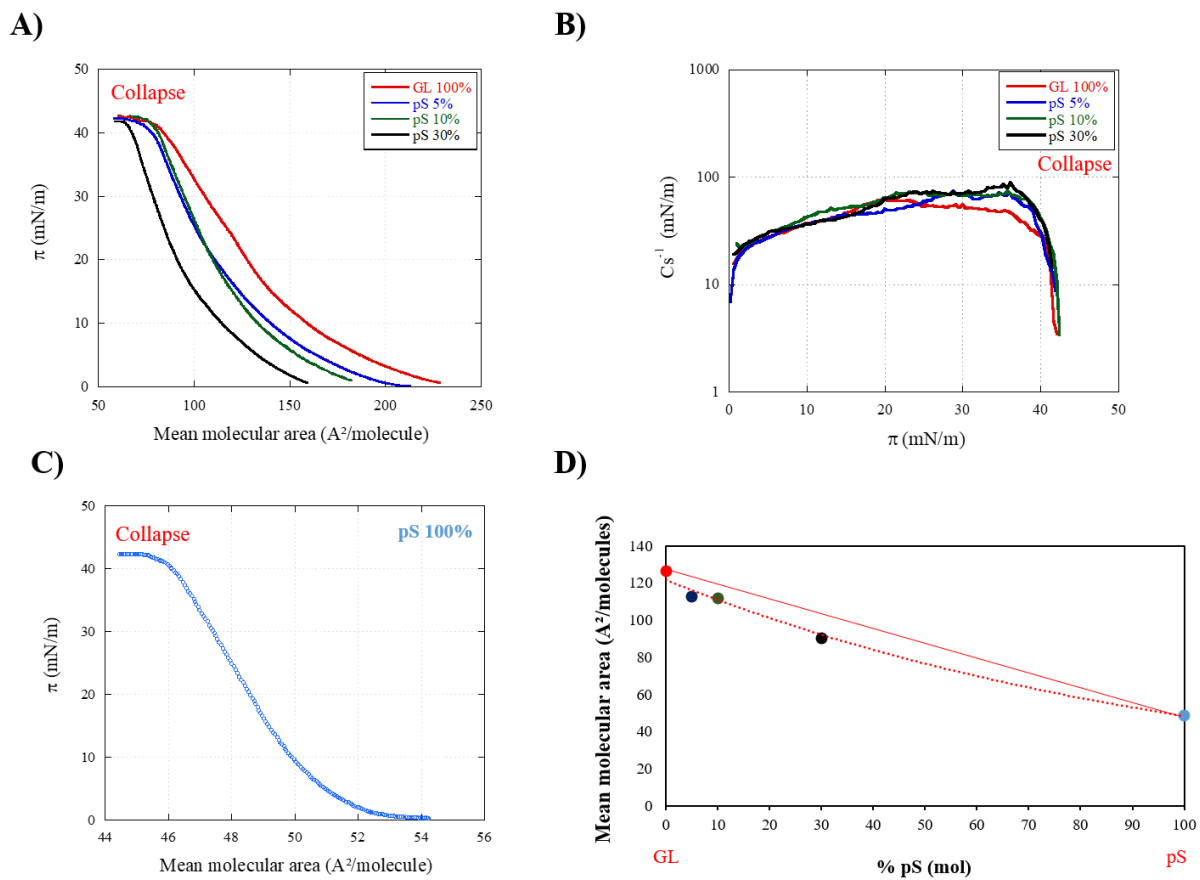
662 **Figure 1**



663

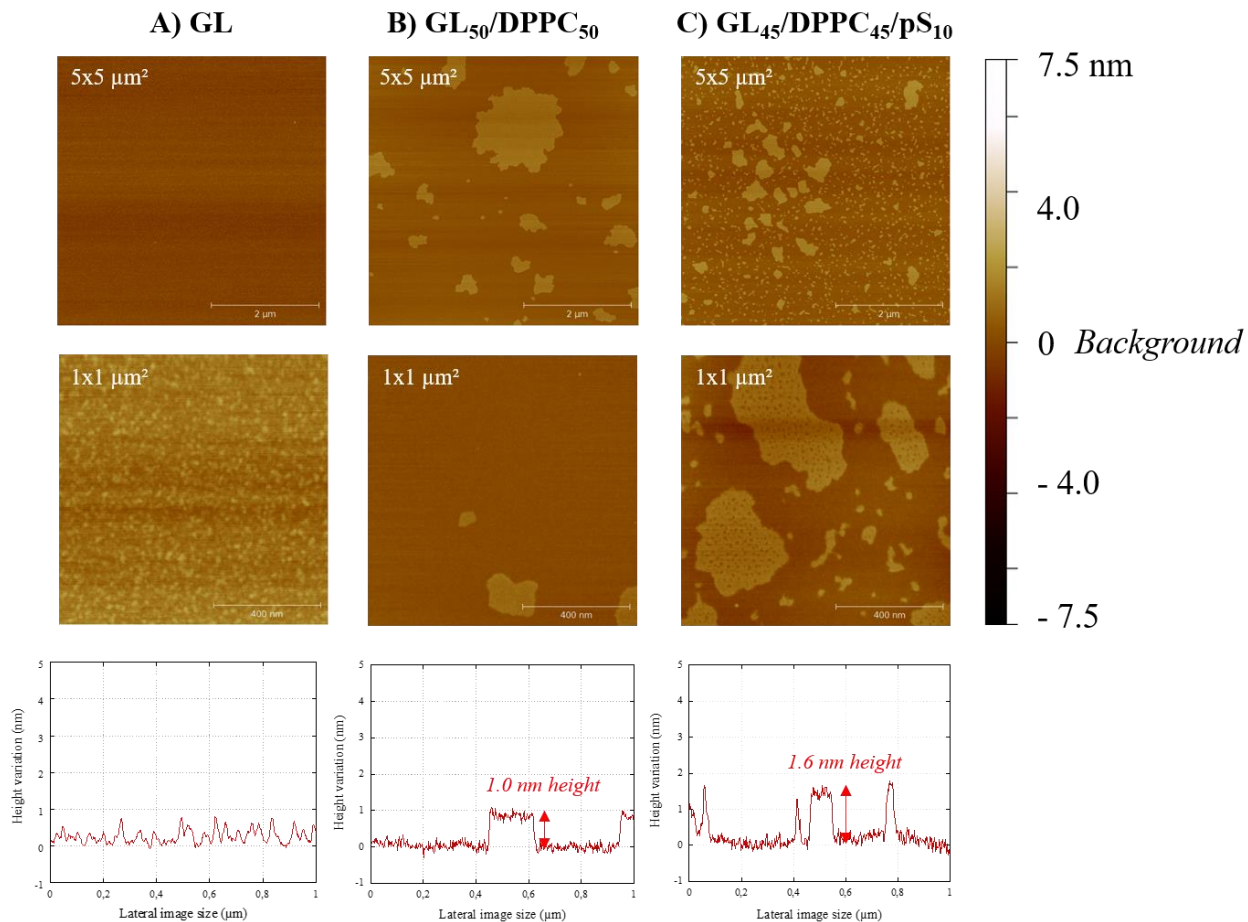
664

665 **Figure 2**



666

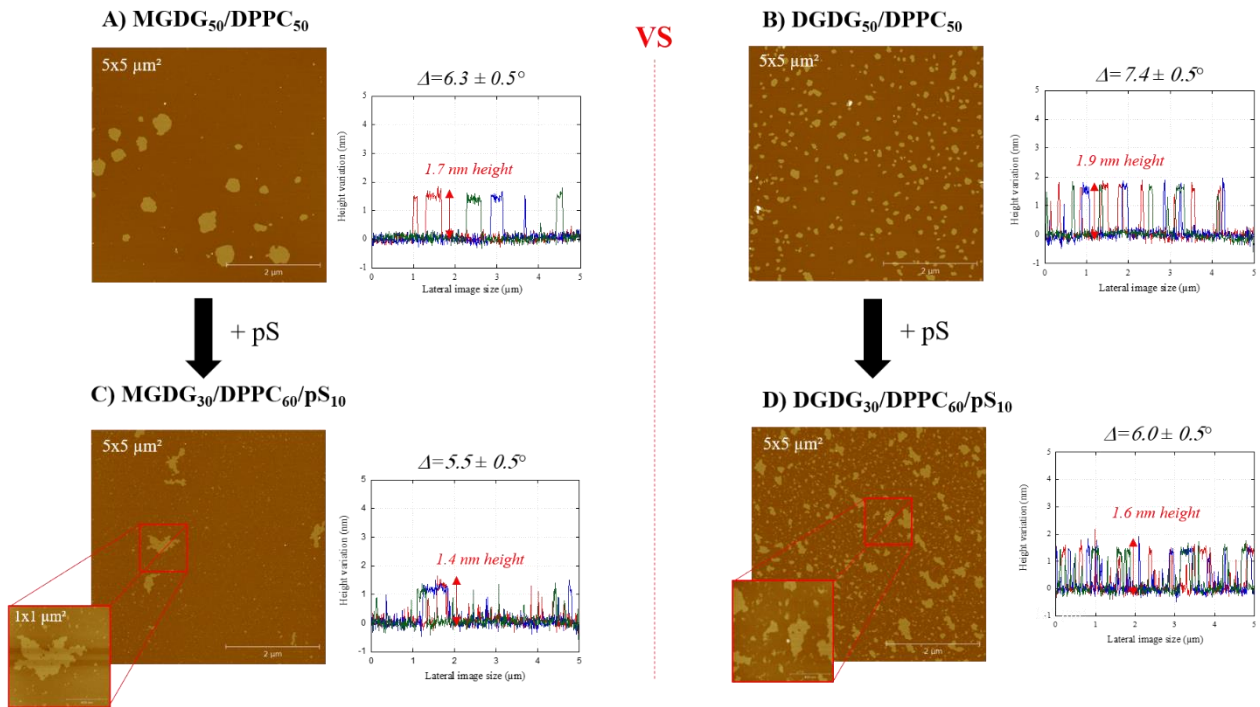
667



669

670

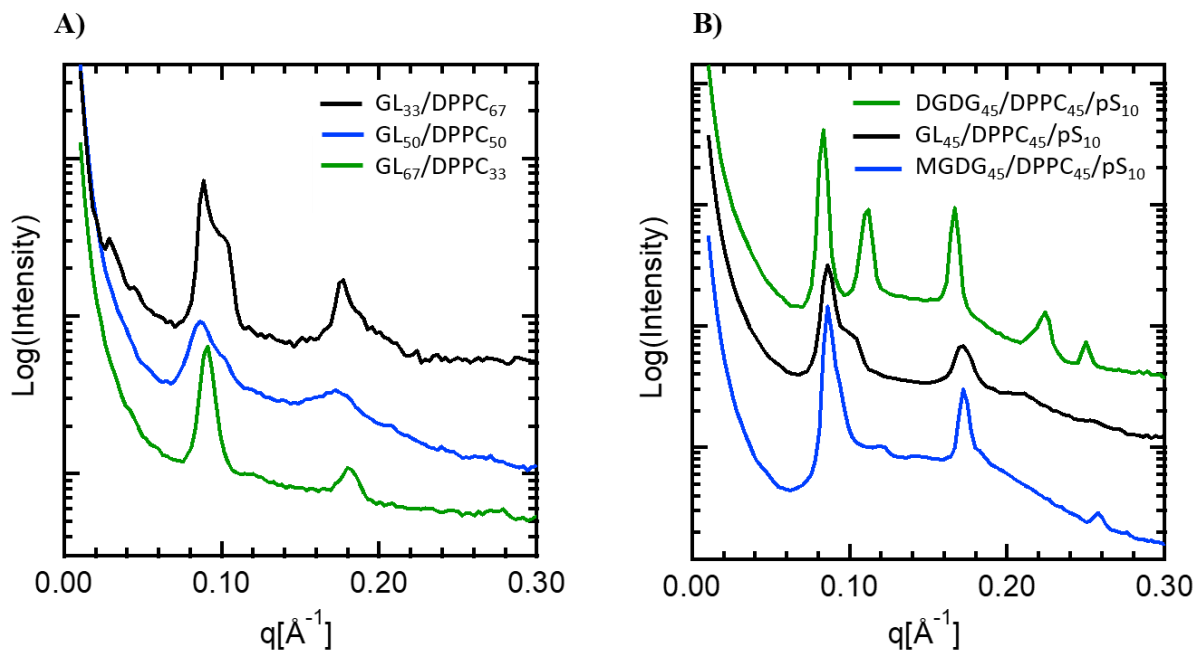
671 **Figure 4**



672

673

674 **Figure 5**



675

676

677 **TABLES**678 **Table 1** - Molar composition of mixed Langmuir monolayers used as model membranes

Monolayer composition	
GL	MGDG/DGDG 60:40 mol/mol
GL ₅₀ /DPPC ₅₀	MGDG/DGDG/DPPC 30:20:50 mol/mol/mol
GL ₄₅ /DPPC ₄₅ /pS ₁₀	MGDG/DGDG/DPPC/pS 27:18:45:10 mol/mol/mol/mol

pS: β -sitosterol, campesterol, brassicasterol 50:40:10 mol/mol/mol

679

680 **Table 2** - Values of π (mN/m), Δ ($^{\circ}$) and limiting molecular area ($\text{\AA}^2/\text{molecule}$) at the collapse of
681 mixed GL, DPPC and pS monolayers

Monolayer composition	π (mN/m)	Δ ($^{\circ}$)	Limiting area ($\text{\AA}^2/\text{molecule}$)
(1) GL	39.9 ± 0.2	7.3 ± 0.5	81.0 ± 0.6
(2) DPPC	55.3 ± 0.2	10.8 ± 0.5	44.1 ± 0.7
(3) GL₅₀/DPPC₅₀	44.1 ± 0.2	8.9 ± 0.5	60.4 ± 1.0
(4) GL₉₀/pS₁₀	41.1 ± 0.1	8.2 ± 0.5	79.5 ± 0.9
(5) GL₄₅/DPPC₄₅/pS₁₀	44.4 ± 0.2	8.6 ± 0.5	55.0 ± 1.7

682 \pm stands for calculated standard deviation on duplicated measurement; for Δ , since the
683 system/instrumentation error is $\pm 0.5^{\circ}$, calculated $\text{SD} \leq 0.5$ were minored by this instrumentation
684 error.

685

686

687 **Table 3** - Ellipsometric angle values of the lipid films at a surface pressure of 20 mN/m at the
688 air/water interface

Monolayer composition	Δ (°)
MGDG	6.3 ± 0.5
DGDG	7.5 ± 0.5
(1) GL	7.5 ± 0.5
(2) GL₅₀/DPPC₅₀	7.1 ± 0.5
(3) GL₄₅/DPPC₄₅/pS₁₀	7.0 ± 0.5

\pm stands for calculated standard deviation on duplicated measurement; the system/instrumentation error is $\pm 0.5^\circ$. Calculated SD ≤ 0.5 were minored by this instrumentation error.

689

690